# Resonant Phase Patterns in a Reaction-Diffusion System

Anna L. Lin, Matthias Bertram, Karl Martinez, and Harry L. Swinney
*Center for Nonlinear Dynamics and Department of Physics, The University of Texas at Austin, Austin, Texas 78712*

Alexandre Ardelea and Graham F. Carey
*CFD Laboratory and ASE/ME Department, The University of Texas at Austin, Austin, Texas 78712*
(Received 22 September 1999)

Resonance regions similar to the Arnol'd tongues found in single oscillator frequency locking are observed in experiments using a spatially extended periodically forced Belousov-Zhabotinsky system. We identify six distinct 2:1 subharmonic resonant patterns and describe them in terms of the position-dependent phase and magnitude of the oscillations. Some experimentally observed features are also found in numerical studies of a forced Brusselator reaction-diffusion model.

PACS numbers: 82.40.Ck, 05.45.Xt, 05.65.+b, 47.54.+r

Frequency locking of a nonlinear oscillator to an external periodic perturbation is exhibited by all physical, chemical, and biological oscillators. The temporal response of a single oscillator to a small amplitude time-periodic stimulus is either quasiperiodic (unlocked) or periodic (locked), depending on the values of the two external control parameters—the forcing amplitude $\gamma$ and the forcing frequency $f$. Larger values of $\gamma$ yield locking over a broader range of detuning from exact resonance. The frequency-amplitude plane shows tongue-shaped regions of resonance ("Arnol'd tongues") and exhibits many of the features of frequency locking for a single oscillator. Entrainment of oscillating systems to external periodic stimuli has been well studied in one-dimensional maps [1], ordinary differential equation models [2], and experiments [3]. The entrainment of spiral tip trajectories in spatially extended excitable systems has also been studied [4]. However, much less is known about the effect of a time-periodic stimulus on spatially extended oscillatory systems such as arrays of Josephson junctions and biological systems with circadian rhythms.

The response of a spatially extended system of oscillators is more complicated than that of a single oscillator since it is possible for different points in the frequency-locked continuum to oscillate with different magnitudes and phases with respect to each other. Previous studies of resonance in periodically forced pattern-forming systems [5–8] did not examine the dependence on both $f$ and $\gamma$, which is the subject of this paper.

We have examined the effect of periodic forcing on a spatially extended system of oscillators, the Belousov-Zhabotinsky (BZ) reaction in a thin gel layer. The photosensitive reaction-diffusion system is forced periodically with spatially uniform, time-periodic pulses of light. We find that the Arnol'd tongue regions observed for single oscillator locking persist in this continuum system. We will describe the observations and then show how different patterns can be distinguished by the phase relation between different points in a pattern. Our quasi-two-dimensional reactor is a thin membrane (0.4 mm thick, 22 mm diameter) that has both faces in contact with continuously refreshed reservoirs of reagents for the BZ reaction [9]. Continuous feeding maintains the medium in a nonequilibrium state. The underlying temporal dynamics in the reactor are oscillatory, and the unforced pattern is traveling spiral waves of the ruthenium catalyst Ru(II) concentration. Regions of higher Ru(II) concentrations appear darker in images.

Figure 1 shows the 2:1 resonance tongue as a function of the applied light intensity $\gamma^2$ and the perturbation frequency $f$; for each data point within the solid lines in Fig. 1 the temporal power spectrum of the intensity time series for any spatial point in the pattern exhibits a large, sharp response at one-half the forcing frequency. The subharmonic 2:1 resonance tongue is discussed here; other resonance tongues will be described elsewhere. The bending of the

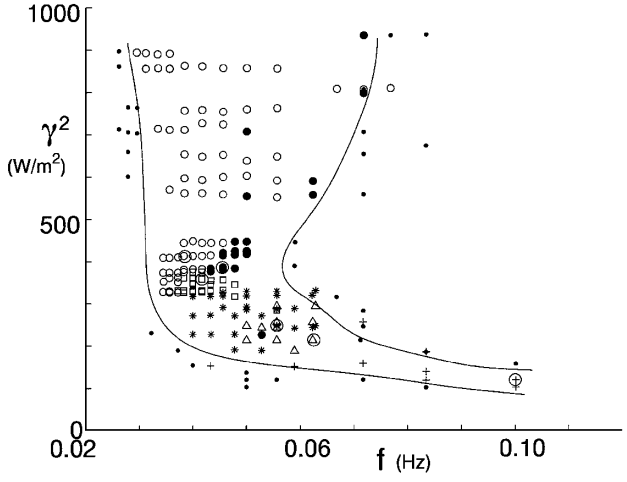


FIG. 1. A 2:1 resonant tongue in the frequency-intensity plane for the experimental system. The patterns (points) within the solid curves resonate at one-half the forcing frequency. The small dots outside the curves are non-2:1-resonant. The perturbation is spatially uniform square-wave light pulses of intensity $\gamma^2$, the square of the light amplitude. See Fig. 2 to connect the symbols and letters to a pattern: + (b); △ (c); * (d); □ (e); ● (f); ○ (g).

 0031-9007/00/84(18)/4240(4)$15.00 

2:1 tongue toward higher frequencies at low amplitude is a characteristic of the BZ reaction—the natural frequency of the oscillations is $\gamma$ dependent. Normalizing the $f$ axis by the natural frequency is not feasible because we cannot accurately measure the homogeneous natural oscillation frequency at low forcing amplitudes. There are places in the control-parameter space shown in Fig. 1 where different symbols overlap because of a slow drift in the parameter values over several months; there is no evidence for multiplicity of pattern states.

Figure 2 shows the different patterns observed within the 2:1 resonance tongue. We distinguish between the patterns with an analysis that uses both the temporal and spatial information; our technique should be useful in quantifying patterns in other systems. We use a finite width frequency filter to extract the complex Fourier amplitude **a** of the temporal subharmonic response of the pattern mode [10]. This is the experimental analog of determining the complex amplitude of the appropriate amplitude equation. Graphs of the complex Fourier amplitude coefficient (at $f/2$) yield information about the relative phase-locked angle and oscillation magnitude of adjacent discretized oscillators in the different patterns.

Figure 3 illustrates the information that can be extracted from the complex Fourier amplitude plots (henceforth referred to as phase portraits). The real space images in the top row show a portion of an unforced rotating spiral wave pattern [Fig. 3(a)] and a subharmonic standing wave pattern [Fig. 3(b)]. The points in each real space image labeled $A, B, C$ and $D, E$ span the dynamic range of the patterns. The plot below each real space image is a corresponding phase portrait. The point labeled $A$ in the complex plane is the complex Fourier amplitude coefficient **a** of the $f/2$ mode for the pixel labeled $A$ in the real space image, and similarly for points $B$–$E$. Through the distribution and connectivity of the Fourier coefficients, the phase portrait shows the distribution of oscillation phases and magnitudes along the dashed line in the real space images. The phase portrait of the unforced spiral pattern in Fig. 3(a) is a circle, indicating that the phase angles of the discretized oscillations in one wavelength of the unforced traveling spiral wave are distributed monotonically from 0 to $2\pi$ and have a uniform magnitude. In contrast, for the standing wave pattern shown in Fig. 3(b), the phase portrait shows that the oscillations remain $\pi$ out of phase on either side of the zero amplitude oscillation node, and the magnitude of the oscillations decreases monotonically as the node is approached.

Pairs of reactor images and phase portraits are shown in Fig. 2 for the different patterns observed within the 2:1 tongue. A histogram of the phase angles is shown directly below each phase portrait. In Figs. 2 and 5, **a** is plotted for all pixels in the image, and the lines connecting adjacent pixels are not shown. The interpretation of the spatial distribution of the oscillations in the unforced rotating spiral in Fig. 2(a) and in the Ising front pattern in Fig. 2(g)

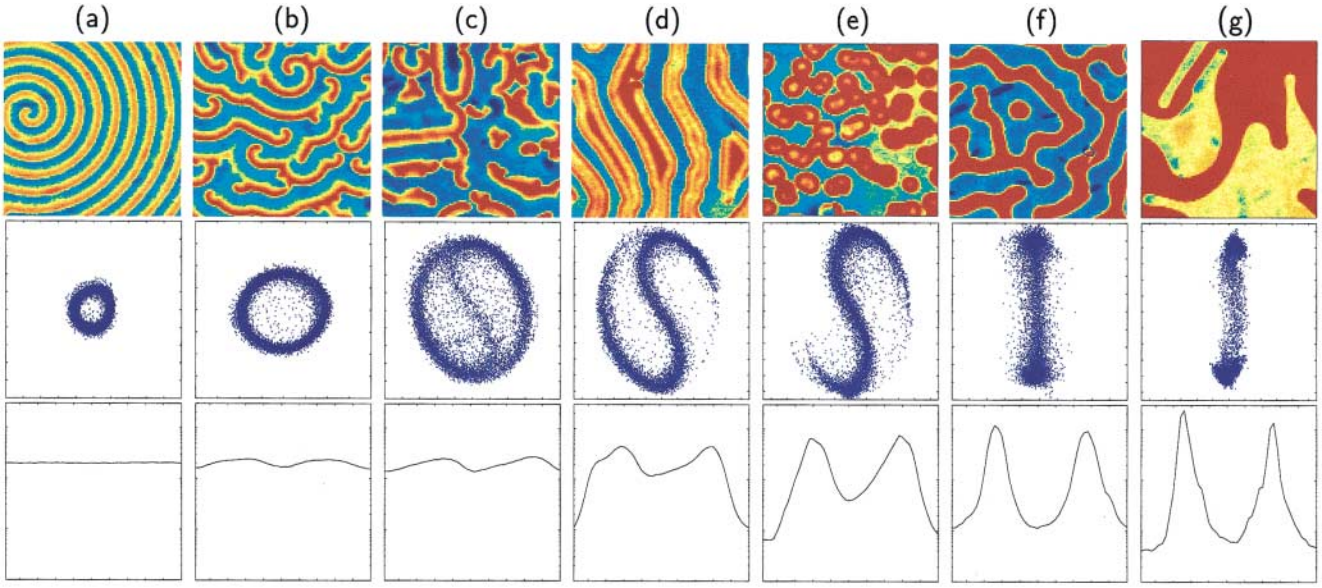


FIG. 2 (color). (top row) Reactor images ($9 \times 9$ mm$^2$) of different observed patterns, presented using a rainbow (false) color map: (a) unforced rotating spiral wave, (b) rotating spiral wave, (c) mixed rotating spiral and standing wave pattern, (d)–(g) qualitatively different standing wave patterns. Patterns (b)–(g) exhibit a 2:1 resonance in the temporal power spectrum of the pattern. (middle row) The complex Fourier amplitude **a** for each image: the abscissa is Re(**a**); the ordinate is Im(**a**). Each point in the complex plane corresponds to the temporal Fourier amplitude **a** of a pixel in the image after frequency demodulation at $f/2$. (bottom row) Histograms of phase angles of all the pixels in each image; the abscissa range is $[0, 2\pi]$ radians and the ordinate range is arbitrary. Chemical conditions are given in [9]. For each pattern the parameter values of $f$(Hz) and $\gamma^2$(W/m$^2$) are, respectively, (a) 0, 0; (b) 0.1000, 119; (c) 0.0625, 214; (d) 0.0556, 248; (e) 0.0417, 358; (f) 0.0455, 386; (g) 0.0385, 412, and correspond to the circled points in Fig. 1.

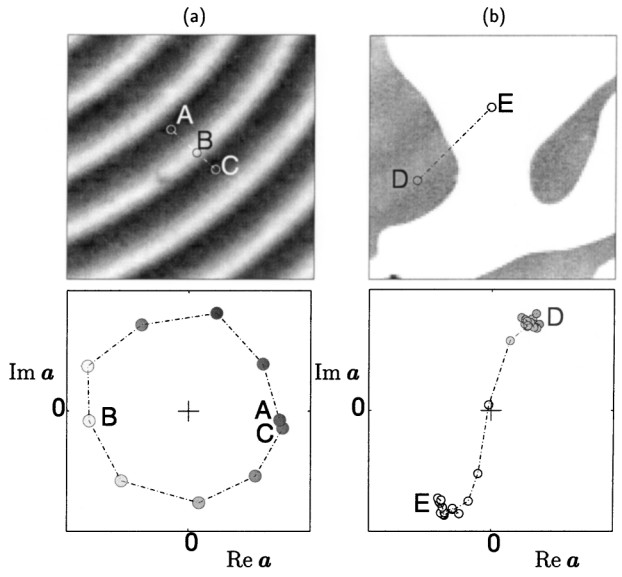


FIG. 3. Reactor images and the corresponding complex Fourier amplitude plots for (a) an unforced rotating spiral pattern ($f = 0$, $\gamma^2 = 0$) and (b) a standing wave Ising front pattern ($f = 0.0380$ Hz, $\gamma^2 = 412\,\mathrm{W/m^2}$). The reactor images are $4.5 \times 4.5$ mm$^2$ and $9 \times 9$ mm$^2$, respectively, and chemical conditions are given in [9].

is the same as that given above for Figs. 3(a) and 3(b), respectively.

The forced complex Ginzburg-Landau (CGL) equation that describes subharmonic 2:1 resonance close to a Hopf bifurcation [6,8] predicts patterns with domains of synchronous oscillations phase shifted by $\pi$. The $\pi$-shifted phase domains are separated from one another by either stationary or traveling phase fronts. The values of the control parameters determine which of these two phase fronts is stable. Our experiments are conducted for conditions far beyond a Hopf bifurcation, but two of the observed patterns, labyrinths and Ising fronts [cf. Figs. 2(f) and 2(g)], exhibit the predicted behavior—they are standing wave patterns with $\pi$-shifted domains of synchronous oscillations connected by stationary fronts.

In contrast, the gradient of phase angles in the pattern in Fig. 2(b) is so small that there are no distinguishable phase fronts. In the 2:1 frequency-locked patterns [Figs. 2(c)–2(e)] there is also a more continuous distribution of the relative oscillation phase, indicated by the "S"-shaped distribution of the Fourier coefficients in the complex plane. The phase-angle distribution is weighted differently around two $\pi$-shifted phases, depending on the values of $\gamma^2$ and $f$, as can be seen more clearly in the histograms plotted in the bottom row of Fig. 2.

We have also conducted numerical simulations of frequency locking in a reaction-diffusion system with Brusselator kinetics, which is not a model of the BZ reaction but is a simple oscillating chemical system with two chemical species,

$$\frac{\partial u}{\partial t} = A - (B + 1)u + [1 + \gamma \sin(2\pi f t)]u^2 v + D_u \nabla^2 u\,, \tag{1}$$

$$\frac{\partial v}{\partial t} = Bu - u^2 v + D_v \nabla^2 v\,, \tag{2}$$

where the parametric forcing term is $\gamma \sin(2\pi f t)u^2 v$, $D_u$ and $D_v$ are the diffusion coefficients of species $u$ and $v$, and $A$ and $B$ are constant parameters corresponding to feed concentrations. Figure 4 shows the 2:1 Arnol'd tongue for this model and for the corresponding homogeneous system ($D_u = D_v = 0$). Other resonant tongues also exist but we present here only the 2:1 case. With diffusion, two-phase spirals [e.g., Fig. 5(b)], labyrinths [Fig. 5(c)], and Ising front [Fig. 5(d)] patterns form within the tongue, while unlocked spiral patterns occur outside the tongue [Fig. 5(a)]. The phase portrait in Fig. 5(b) shows no zero crossings at the phase fronts (no nodes), indicating that the pattern is a traveling wave (a Bloch spiral [8]). The phase of the oscillations varies continuously as one passes from one phase-synchronous domain to the other. In contrast, the phase portraits of the standing wave patterns in Figs. 5(c) and 5(d) show that the phase angle remains fixed and the oscillation magnitude monotonically decreases as the node of a phase front is approached; the phase angle abruptly changes sign (from $-\pi$ to $\pi$) at the node. This type of phase front is also observed in the laboratory system; see Figs. 2(f) and 2(g). While we do not find a one-to-one correspondence between the simulation and the experimental patterns, we note that we have not conducted a complete exploration of either system's multiparameter space where other patterns may exist.

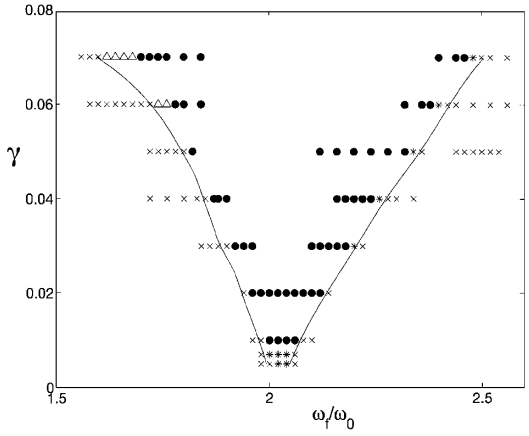


FIG. 4. A 2:1 Arnol'd tongue for the Brusselator model with parametric forcing ($A = 0.5$, $B = 1.5$, $D_u = 0.2D_v$), where $f_0 = 0.41$ is the natural frequency of the unforced, homogeneous system. Lines show the locked-unlocked transition in the *homogeneous* case [$D_u = D_v = 0$ in Eqs. (1) and (2)]. Symbols represent the case with diffusion: (×) unlocked rotating spirals, (*) traveling (Bloch) phase fronts, (△) labyrinths, (●) stationary (Ising) phase fronts. The tongue for the reaction-diffusion system is slightly narrower than that for the homogeneous system.

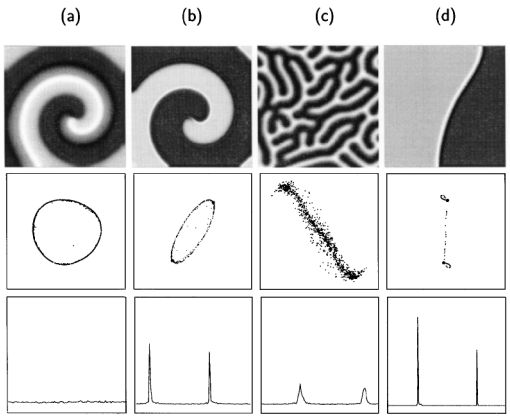


FIG. 5. (top row) Patterns in the Brusselator model: (a) unlocked rotating spiral wave, (b) two-phase spiral, (c) labyrinth, (d) Ising front pattern. (middle row) Fourier amplitude complex plane phase portraits. (bottom row) Histograms of phase angle for all the pixels in each image. In all cases, values for the parameters are $A = 0.5$, $B = 1.5$, and the initial conditions are perpendicular spatial gradients in $U$ and $V$. Values of the parameters $f/f_0$ and $\gamma$ are, respectively, (a) 1.58, 0.05; (b) 2.12, 0.05; (c) 2.40, 0.06; (d) 1.66, 0.07. See Fig. 2 caption for ordinate and abscissa axis labels.

In conclusion, in both laboratory experiments and a reaction-diffusion model we have found a resonant tongue structure that is similar to the well-studied Arnol'd tongues found in low-dimensional systems (maps and ordinary differential equations). The frequency-locked patterns in the experiment and model fit the selection criteria predicted by an analysis of the CGL equation, for certain ranges of the parameters $f$ and $\gamma$. Additionally, some of the experimental resonant patterns show more complicated dynamics, e.g., a continuous distribution of phase-locked angle, resulting in no definable phase fronts. These observations provide a description of the self-organizing behavior of an oscillatory reaction-diffusion continuum exposed to time-periodic external perturbation.

We thank E. Meron, A. Hagberg, V. Petrov, A. Pardhanani, and W. McCormick for discussions and assistance. We acknowledge the support of the Engineering Research Program of the Office of Basic Energy Sciences of the U.S. Department of Energy, the Robert A. Welch Foundation, the Binational Science Foundation, a State of Texas Advanced Technology Program Grant (ATP 221), and an equipment grant from Intel.

[1] M. H. Jensen, P. Bak, and T. Bohr, Phys. Rev. Lett. **50**, 1637 (1983); P. Bak, Phys. Today **39**, No. 12, 38 (1986); R. E. Ecke, J. D. Farmer, and D. K. Umberger, Nonlinearity **2**, 196 (1989); M. Krupa and M. Roberts, Physica (Amsterdam) **57D**, 435 (1992); L. Glass and J. Sun, Phys. Rev. E **50**, 5077 (1994).

[2] G. E. Tsarouhas and J. Ross, J. Chem. Phys. **89**, 5720 (1988); C. Knudsen, J. Sturis, and J. Thomsen, Phys. Rev. A **44**, 3503 (1991).

[3] L. Pivka, A. L. Zheleznyak, and L. O. Chua, Int. J. Bifurcation Chaos Appl. Sci. Eng. **4**, 1753 (1994); L. Glass, Phys. Today **49**, No. 8, 40 (1996).

[4] M. Braune and H. Engel, Chem. Phys. Lett. **211**, 534 (1993); O. Steinbock, V. Zykov, and S. C. Müller, Nature (London) **366**, 322 (1993); V. N. Biktashev and A. V. Holden, Chaos Solitons Fractals **5**, 575 (1995); R.-M. Mantel and D. Barkley, Phys. Rev. E **54**, 4791 (1996); V. Hakim and A. Karma, Phys. Rev. E **60**, 5073 (1999).

[5] A. Chiffaudel and S. Fauve, Phys. Rev. A **35**, 4004 (1987).

[6] P. Coullet, J. Lega, B. Houchmanzadeh, and J. Lajzerowicz, Phys. Rev. Lett. **65**, 1352 (1990).

[7] V. Petrov, Q. Ouyang, and H. L. Swinney, Nature (London) **388**, 655 (1997).

[8] C. Elphick, A. Hagberg, and E. Meron, Phys. Rev. E **59**, 5285 (1999).

[9] Chemical concentrations reservoir I: $0.22M$ malonic acid, $0.2M$ NaBr, $0.264M$ $KBrO_3$, $0.8M$ $H_2SO_4$; Reservoir II: $0.184M$ $KBrO_3$, $1 \times 10^{-3}M$ Tris(2,2′-bipyridyl)dichlororuthenium(II)hexahydrate, $0.8M$ $H_2SO_4$. Volume of reservoir, 8.3 ml. Flow rate through reservoir I was 20 ml/h; reservoir II, 5 ml/h.

[10] In temporal frequency space, we convolve the spectrum of coefficients for each spatial point with the spectrum of coefficients from a sinc function of width $f/2$, thus removing higher order harmonics. We then apply a Fourier transform to return to the time domain.